

# DISCOVERY OF A VERY BRIGHT AND INTRINSICALLY VERY LUMINOUS, STRONGLY LENSED LYMAN ALPHA EMITTING GALAXY AT $z=2.82$ IN THE BOSS EMISSION-LINE LENS SURVEY<sup>†</sup>

RUI MARQUES-CHAVES<sup>1,2</sup>, ISMAEL PÉREZ-FOURNON<sup>1,2</sup>, YIPING SHU<sup>3</sup>, PALOMA I. MARTÍNEZ-NAVAJAS<sup>1,2</sup>,  
ADAM S. BOLTON<sup>4, 5</sup>, CHRISTOPHER S. KOCHANÉK<sup>6</sup>, MASAMUNE OGURI<sup>7, 8, 9</sup>, ZHENG ZHENG<sup>4</sup>, SHUDE MAO<sup>10, 3, 11</sup>,  
ANTONIO D. MONTERO-DORTA<sup>4</sup>, MATTHEW A. CORNACHIONE<sup>4</sup>, AND JOEL R. BROWNSTEIN<sup>4</sup>

*Draft version May 24, 2022*

## ABSTRACT

We report the discovery of a very bright ( $r = 20.16$ ), highly magnified, and yet intrinsically very luminous Ly $\alpha$  emitter (LAE) at  $z = 2.82$ . This system comprises four images in the observer plane with a maximum separation of  $\sim 6''$  and it is lensed by a  $z = 0.55$  massive early-type galaxy. It was initially identified in the Baryon Oscillation Spectroscopic Survey (BOSS) Emission-Line Lens Survey for GALaxy-Ly $\alpha$  Emitter sYstems (BELLS GALLERY) survey, and follow-up imaging and spectroscopic observations using the *Gran Telescopio Canarias* (GTC) and *William Herschel Telescope* (WHT) confirmed the lensing nature of this system. A lens model using a singular isothermal ellipsoid in an external shear field reproduces quite well the main features of the system, yielding an Einstein radius of  $2''.95 \pm 0''.10$ , and a total magnification factor for the LAE of  $8.8 \pm 0.4$ . This LAE is one of the brightest and most luminous galaxy-galaxy strong lenses known. We present initial imaging and spectroscopy showing the basic physical and morphological properties of this lensed system.

*Subject headings:* cosmology: observations — galaxies: evolution — gravitational lensing: strong — galaxies: individual (BG1429+1202)

## 1. INTRODUCTION

The study of the physical properties of typical  $L^*$  high-redshift galaxies has been limited by their faintness ( $r \simeq 24.5$  at  $z \sim 3$ ), even for 8-/10-m class telescopes. Over the past years the properties of these high-redshift galaxies have been studied by building large samples of hundreds to thousands individual spectra to construct high signal-to-noise (S/N) composite spectra (e.g. Shapley et al. 2003). Although these techniques have been very successful, they require a large amount of observ-

ing time and only probe the average physical properties of these galaxies. Another way to study in detail high-redshift galaxies is using the fortuitous alignments with foreground massive structures which provide natural magnification and associated amplification produced by strong gravitational lensing. Hundreds of strongly lensed galaxies have been discovered in the last years employing various observational techniques, mainly from optical to radio. However, only a handful of optically very bright ( $r \sim 20$ ), strongly magnified high-redshift galaxies, have been discovered so far (Yee et al. 1996; Al- lam et al. 2007; Smail et al. 2007; Belokurov et al. 2007; Lin et al. 2009; Dahle et al. 2016) allowing detailed spectroscopic studies of their individual properties, such as stellar populations, chemical composition, and kinematics of the interstellar medium (e.g., Pettini et al. 2000, 2002; Quider et al. 2009, 2010; Dessauges-Zavadsky et al. 2010).

In this Letter, we report the discovery of a bright ( $r \sim 20$ ) quadruply gravitationally lensed Ly $\alpha$  emitter (LAE). We provide the first physical and morphological analysis of the lensing galaxy and the lensed LAE. Throughout the Letter, we adopt a cosmology with  $\Omega_m = 0.274$ ,  $\Omega_\Lambda = 0.726$  and  $H_0 = 70 \text{ km s}^{-1} \text{ Mpc}^{-1}$ . All quoted magnitudes are in the AB system.

## 2. DISCOVERY AND FOLLOW-UP

In the past years, by searching for secondary emission lines in the spectra of massive elliptical galaxies within the database of the Sloan Digital Sky Survey (SDSS: York et al. 2000), the Sloan Lens ACS Survey (SLACS: e.g., Bolton et al. 2006, 2008), and the Baryon Oscillation Spectroscopic Survey (BOSS) Emission-Line Lens Survey (BELLS: Brownstein et al. 2012) have discovered over 100 lensed star-forming galaxies at moderate redshifts ( $z \sim 1$ ). Very recently, by applying spectroscopic selection techniques similar to SLACS and BELLS, but

<sup>†</sup> Based on observations made with the Gran Telescopio Canarias (GTC) and William Herschel Telescope (WHT), in the Spanish Observatorio del Roque de los Muchachos of the IAC, under Directors Discretionary Time (DDT programs IDs: GTC2016-054 and DDT2016-077).

<sup>1</sup> Instituto de Astrofísica de Canarias, C/Vía Láctea, s/n, E-38205 San Cristóbal de La Laguna, Tenerife, Spain

<sup>2</sup> Universidad de La Laguna, Dpto. Astrofísica, E-38206 La Laguna, Tenerife, Spain

<sup>3</sup> National Astronomical Observatories, Chinese Academy of Sciences, A20 Datun Rd., Chaoyang District, Beijing 100012, China

<sup>4</sup> Department of Physics and Astronomy, University of Utah, 115 South 1400 East, Salt Lake City, UT 84112, USA

<sup>5</sup> National Optical Astronomy Observatory, 950 N. Cherry Ave., Tucson, AZ 85719 USA

<sup>6</sup> Department of Astronomy & Center for Cosmology and Astroparticle Physics, Ohio State University, Columbus, OH 43210, USA

<sup>7</sup> Research Center for the Early Universe, University of Tokyo, 7-3-1 Hongo, Bunkyo-ku, Tokyo 113-0033, Japan

<sup>8</sup> Department of Physics, University of Tokyo, 7-3-1 Hongo, Bunkyo-ku, Tokyo 113-0033, Japan

<sup>9</sup> Kavli Institute for the Physics and Mathematics of the Universe (Kavli IPMU, WPI), University of Tokyo, Chiba 277-8583, Japan

<sup>10</sup> Physics Department and Tsinghua Centre for Astrophysics, Tsinghua University, Beijing 100084, China

<sup>11</sup> Jodrell Bank Centre for Astrophysics, School of Physics and Astronomy, The University of Manchester, Oxford Road, Manchester M13 9PL, UK

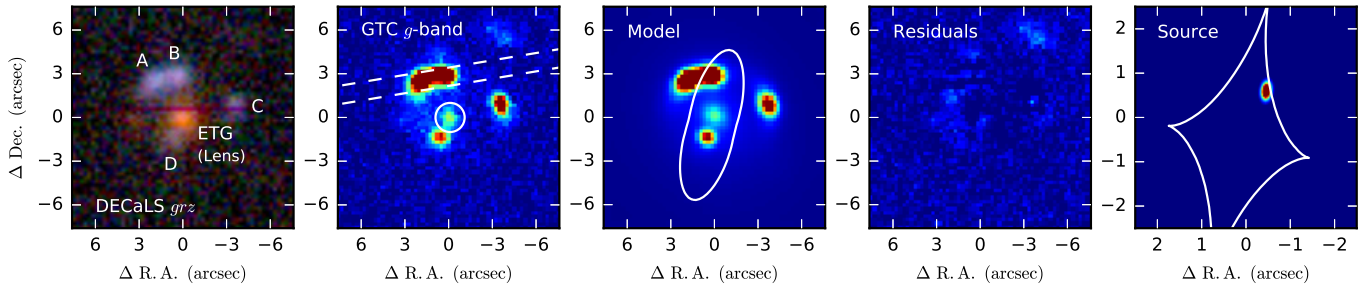


FIG. 1.— From left to right: DECaLS *grz* color image of the lens system; GTC/OSIRIS *g*-band image showing the orientation of the WHT/ACAM and GTC/OSIRIS long slits (white dashed lines) and the position of the spectroscopic 1''-radius BOSS fibre (white circle); predicted lensed and foreground images with the critical line; final residuals from the best-fit model; and position of the LAE in the source plane relative to the caustic. All the images are centered on the lensing galaxy and oriented such that North is up and East is to the left.

adapted to high-redshift Ly $\alpha$  emission, Shu et al. (2016a) identified a new sample of 187 high-probability lensed LAE candidate systems at  $2 < z_{\text{LAE}} < 3$ , the BOSS Emission-Line Lens Survey for GALaxy-Ly $\alpha$  Emitter sYstems (BELLS GALLERY) survey, selected from the final data release (DR12) of the BOSS (Dawson et al. 2013) of the SDSS-III (Eisenstein et al. 2011). Of these, 21 highest-quality candidates were recently observed with the *Hubble Space Telescope* (HST) and the first results were presented in Shu et al. (2016b).

By visual inspection of SDSS and DECaLS<sup>13</sup> color images of the BELLS GALLERY sample, we found one candidate showing bluish features  $\simeq 3''.3$  from the  $z = 0.5531$  massive early-type galaxy, SDSS J142954.80+120235.6 (hereafter ETG). Its BOSS spectrum (Plate-MJD-Fiber: 5463-56003-121) shows a secondary emission line at  $4652\text{\AA}$  (Ly $\alpha$  at  $z = 2.8253$ ; Shu et al. 2016a). The positions of the bluish features with respect to the ETG are consistent with a *fold* lensing configuration: a bright lensed image pair, A and B (with a separation of  $\simeq 1''.5$ ), and two fainter images, C and D (see Fig. 1). The lensed image pair, A and B, is identified in SDSS as a single source, SDSS J142954.88+120238.3 (hereafter BG1429+1202 for the lensed LAE, where BG stands for BELLS GALLERY), showing blue colors in DECaLS and SDSS bands (Table 1). The lensed A and B images are also detected in the UKIRT Infrared Deep Sky Survey (UKIDSS: Lawrence et al. 2007) Large Area Survey (LAS), only in Y-band with  $21.06 \pm 0.19$  mag and  $21.12 \pm 0.20$  mag, respectively.

We carried out Director Discretionary Time (DDT) for optical imaging and long-slit spectroscopic observations on 2016 June 29 using the Auxiliary-port Camera (ACAM: Benn et al. 2008) at the *William Herschel Telescope* (WHT) to confirm the lensing nature of this LAE. The ACAM long-slit was oriented at sky position angle (PA) =  $103^\circ.35$ , and positioned so as to encompass the two brightest lensed images, A and B, as shown in Fig. 1. Despite the bad seeing conditions that night ( $\sim 4''$  FWHM), we could confirm the lensing nature of this system with the detection in the long-slit spectrum of strong rest-frame UV continuum (with Si IV and C IV in absorption) and Ly $\alpha$  emission at a redshift  $z = 2.823 \pm 0.008$ , in agreement with the redshift of the Ly $\alpha$  detected in

TABLE 1  
PROPERTIES OF THE SYSTEM

ID	R.A. <sup>(1)</sup> (J2000.0)	Dec. <sup>(1)</sup> (J2000.0)	<i>g</i> <sup>(2)</sup>	<i>r</i> <sup>(3)</sup>	<i>z</i> <sup>(4)</sup>
ETG	14:29:54.806	+12:02:35.53	22.88	20.51	19.00
			$\pm 0.12$	$\pm 0.07$	$\pm 0.10$
A <sup>(5)</sup>	14:29:54.936	+12:02:38.23	21.48	21.23	21.32
			$\pm 0.08$	$\pm 0.03$	$\pm 0.04$
B <sup>(5)</sup>	14:29:54.831	+12:02:38.48	21.64	21.34	21.31
			$\pm 0.08$	$\pm 0.03$	$\pm 0.04$
C	14:29:54.570	+12:02:36.69	22.27	22.22	22.02
			$\pm 0.09$	$\pm 0.08$	$\pm 0.09$
D	14:29:54.848	+12:02:34.24	22.57	22.30	21.85
			$\pm 0.11$	$\pm 0.10$	$\pm 0.11$
Total LAE			20.40	20.16	20.07

NOTE. — (1) positions with  $0''.11$  astrometric r.m.s. using GAIA DR1 (Gaia Collaboration et al. 2016); (2) photometry and  $1\sigma$  errors from the GTC/OSIRIS *g*-band image; (3) and (4) photometry and  $1\sigma$  errors from the DECaLS DR2 Tractor catalog, except for the lens which were taken from the SDSS DR12 due to image artifacts in DECaLS co-adds, and (5) the lensed images A and B were deblended using GALFIT (Peng et al. 2002). The magnitudes listed have not been corrected for the Galactic dust extinction, which is 0.104, 0.072, and 0.040 mag for *g*, *r*, and *z*, respectively (Schlafly & Finkbeiner 2011).

the BOSS fiber spectrum, likely from the lensed image D (see Fig. 1).

We observed again BG1429+1202 on 2016 July 29, this time in very good seeing conditions ( $\simeq 0''.75$  FWHM, measured in the 330 s *g*-band acquisition image), using the Optical System for Imaging and low-Intermediate-Resolution Integrated Spectroscopy camera (OSIRIS<sup>14</sup>) on the *Gran Telescopio Canarias* (GTC). We used the R1000B grism, which provides a spectral coverage of 3630 - 7500  $\text{\AA}$  (950 - 1960  $\text{\AA}$ , rest-frame) and a dispersion of  $2.12 \text{ \AA px}^{-1}$ . The OSIRIS  $1''.2$  wide long-slit was oriented in the same PA used in the WHT/ACAM spectroscopic observations (Fig. 1). Given this configuration, the corresponding spectral resolution is  $\simeq 8 \text{ \AA}$  (or  $\simeq 500 \text{ km s}^{-1}$  FWHM). The total integration time was 44 minutes, split into  $4 \times 660$  s. The data were reduced with IRAF and PYTHON tasks.

### 3. ANALYSIS AND DISCUSSION

<sup>13</sup> Dark Energy Camera Legacy Survey: <http://legacysurvey.org/decacls/>

<sup>14</sup> <http://www.gtc.iac.es/instruments/osiris/>

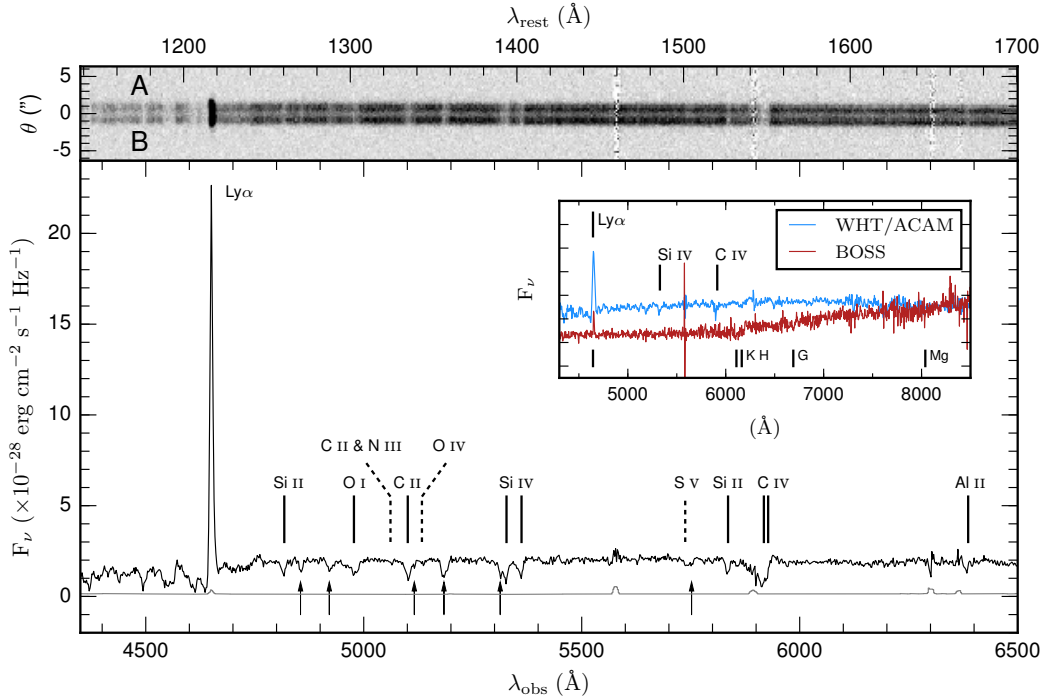


FIG. 2.— GTC/OSIRIS spectrum of BG1429+1202 (black solid line) and its  $1\sigma$  error (grey solid line). Ticks mark the positions of the strong interstellar absorption features (solid lines) and photospheric lines (dashed lines) of BG1429+1202, as well as other absorption features related to intervening systems at lower redshifts (black solid arrows). The 2D spectrum is also shown on the top. In the inset panel we show the BOSS and WHT spectra with the positions of the  $\text{Ly}\alpha$  emission as well as the absorption features related to the ETG at  $z = 0.5531$  from the BOSS fiber spectrum.

### 3.1. Source Properties

The rest-frame UV spectrum of the brightest lensed images A and B, is shown in Fig. 2. Despite the relatively short exposure time, the achieved high S/N GTC/OSIRIS spectrum ( $\sim 25$  in the continuum) shows a strong  $\text{Ly}\alpha$  emission, and a series of strong absorption lines, similar to those seen in the composite spectrum of hundreds  $z \sim 3$  Lyman break galaxies (LBGs) (Shapley et al. 2003). The strongest absorption features are associated to the interstellar medium and stellar winds in a variety of ionization states, from neutral (O I) to highly ionized species (Si IV or C IV). High ionization features with a strong P Cygni profile are seen both in C IV  $\lambda 1548$ , 1550 and Al III  $\lambda 1854$ , 1862 doublets, which is indicative of stellar winds from very young massive stars. However, we identify additional absorption features unrelated to BG1429+1202 (nine absorption features associated to an intervening metal-line system at  $z_{\text{abs}} = 2.179 \pm 0.001$ , and one broad absorption line at  $5183\text{\AA}$  with an observed equivalent width  $W_{\text{obs}} = 6.95 \pm 0.2\text{\AA}$  remains unidentified). Analysis of the spectra for the individual lensed images A and B shows no differences in the profiles of the absorption features neither evidence for velocity offsets between them, as expected if they are both images of the same background source. The same happens to their rest-frame UV slope,  $\beta$ , which is essentially flat in  $F_{\nu}$ . Adopting a simple power-law approximation for the UV spectral range  $F_{\lambda} \propto \lambda^{\beta}$  and using the observed  $r$  and  $z$  magnitudes ( $\sim 1600 - 2400\text{\AA}$  rest-frame), we derive  $\beta = -2.1 \pm 0.1$ , which implies an effective UV extinction  $A_{1600} \sim 0.6$  or  $E(B - V) \sim 0.13$ , reflecting modest dust content (Calzetti et al. 2000).

We identified several photospheric absorption features,

from which we derived the systemic redshift  $z_{\text{sys}} = 2.8224 \pm 0.0013$  using the cleanest among them: O IV  $\lambda 1343$ , and a close blend of C II and N III at  $\lambda 1324$ .

The  $\text{Ly}\alpha$  emission line has an observed (A + B) flux of  $F_{\text{Ly}\alpha} = (2.1 \pm 0.3) \times 10^{-15} \text{ erg s}^{-1} \text{ cm}^{-2}$ , much higher than the  $\text{Ly}\alpha$  flux measured within the  $1''$ -radius BOSS fibre ( $F_{\text{Ly}\alpha}^{\text{BOSS}} = 0.256 \times 10^{-15} \text{ erg s}^{-1} \text{ cm}^{-2}$ ). The measured rest-frame equivalent width of  $\text{Ly}\alpha$  is  $W_0^{\text{Ly}\alpha} = 39 \pm 15\text{\AA}$ . The errors reflect the uncertainty in the determination of the stellar continuum redward of  $\text{Ly}\alpha$ . Although the line appears unresolved in our low resolution spectrum ( $\text{FWHM} \simeq 500 \text{ km s}^{-1}$ ), it is resolved in the BOSS spectrum. Fitting a Gaussian to the BOSS  $\text{Ly}\alpha$  line, we measured a FWHM of  $382 \pm 50 \text{ km s}^{-1}$ , after accounting for the instrumental broadening. The nebular C III]  $\lambda 1906$ , 1908 doublet is also detected in emission but with low significance ( $4\sigma$ ) and not resolved in our GTC/OSIRIS spectrum. This galaxy can be classified as a LAE, given the rest-frame equivalent width and the velocity width of the  $\text{Ly}\alpha$  line (e.g., Ouchi et al. 2008). From our spectrum and available photometric data we do not detect evidence of any AGN contribution. However, a more extensive characterization awaits higher spatial resolution imaging and multi-wavelength photometry.

A careful analysis of the kinematics goes beyond the present Letter given the low spectral resolution of these data. However, the high S/N of the GTC/OSIRIS spectrum allows us to detect differences in the kinematics of the  $\text{Ly}\alpha$  emission and interstellar features. Fig. 3 (left panel) shows velocity plots of the  $\text{Ly}\alpha$  emission line and several normalized interstellar absorption lines, relative to  $z_{\text{sys}}$ . The  $\text{Ly}\alpha$  emission has its peak redshifted with

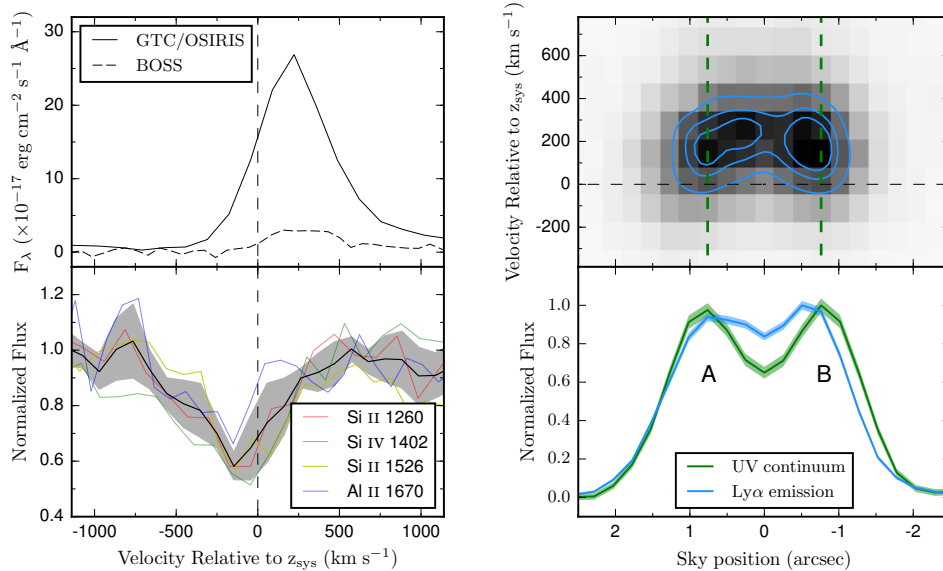


FIG. 3.— Left: GTC/OSIRIS and BOSS Ly $\alpha$  emission (upper panel) and interstellar absorption features (lower panel) on rest velocity frame. The Ly $\alpha$  emission appears to be redshifted,  $v_{\text{Ly}\alpha} \sim +200 \text{ km s}^{-1}$ , while the interstellar absorption lines are blueshifted by  $v_{\text{abs}} \sim -150 \text{ km s}^{-1}$  (mean profile in black with the standard deviation in grey shadow). Right: 2D Ly $\alpha$  emission in the position-velocity plane (upper panel) where a spatial gradient of velocity is seen in both A and B images. In the lower panel we show the normalized spatial profiles of the rest-frame UV continuum (green line) and Ly $\alpha$  emission (blue line). The shaded regions show the  $1\sigma$  errors of the spatial profiles. The Ly $\alpha$  emission appears more extended between A and B, than the rest-frame UV continuum.

a velocity  $v_{\text{Ly}\alpha} \sim +200 \text{ km s}^{-1}$ , while the interstellar absorption lines appear blueshifted by  $\sim -150 \text{ km s}^{-1}$ , which is consistent with galaxy-scale outflows of material from the galaxy in the form a wind, similar to those seen in other star-forming galaxies at  $z \sim 3$  (Shapley et al. 2003).

We also notice that a spatial gradient of the Ly $\alpha$  velocity is present in the 2D spectrum (Fig. 3, right upper panel). This velocity structure is seen both in A and B but appears mirrored, as expected for those images in this system as A and B images straddle the fold critical curve (see figure 1). We checked carefully the 2D spectrum to see if this pattern is present in other lines, but we found none with this signature. The 1D spatial distribution of Ly $\alpha$  is also compared with that of the rest-frame UV continuum (Fig. 3, right lower panel). The Ly $\alpha$  emission appears more extended in the inner region between A and B, than the UV continuum. Deeper and higher spatial resolution observations are needed to constrain the Ly $\alpha$  and UV continuum spatial distributions.

### 3.2. Lens Model

To interpret the properties of the lensed system in more detail, we used the 330 s GTC/OSIRIS  $g$ -band image obtained in  $\simeq 0.75''$  FWHM seeing for accurate lens modeling. As shown in Fig. 1, the lens system comprises four images forming a so-called *fold* configuration, when the source lies very close to a *fold* caustic. Similar to previous works (Bolton et al. 2008; Brownstein et al. 2012; Shu et al. 2015, 2016b,c), we have developed a lens model using a non-linear optimizer, consisting on minimizing a  $\chi^2$  function using the Levenberg-Marquardt algorithm with the LMFIT package (Newville et al. 2014), where the observational data is compared to the model (see Shu et al. 2016b, for details). The foreground-light is modeled us-

ing the elliptical Sérsic profile and similar to Shu et al. (2015, 2016b,c) its subtraction is performed jointly with the lens modeling. The lens model includes a mass distribution of the foreground lens parameterized as a singular isothermal ellipsoid (SIE), and an additional external shear is included to model the higher-order effect from the environment. The surface brightness distribution of the background source is reconstructed parametrically using an elliptical Sérsic model. The foreground-light model is combined with the predicted lensed images and convolved with the point-spread function (PSF) which was modeled with a star in the GTC/OSIRIS  $g$ -band field-of-view.

The best fit lens model ( $\chi^2/\text{dof} = 3494/3709$ ) predicts for the lens an Einstein radius  $b_{\text{SIE}} = 2''.95 \pm 0''.10$ , minor-to-major axis ratio  $q = 0.34$  and a position angle P.A. =  $165.5^\circ$ . The strength and position angle of the external shear is  $\gamma = 0.059 \pm 0.008$  and  $\phi_\gamma = 89.9^\circ$ , respectively. The characteristic lensing velocity dispersion defined as  $\sigma_{\text{SIE}} = c\sqrt{\frac{b_{\text{SIE}}}{4\pi} \frac{D_L}{D_{\text{LS}}}}$  is  $390 \pm 6 \text{ km s}^{-1}$ , where  $D_{\text{LS}}$  and  $D_S$  are the angular diameter distances from the lens and the observer to the source, respectively. We also find a minor-to-major axis ratio of the SIE component (0.34), smaller than that of the light distribution suggested by the  $g$ -band model result (0.85). The lensing velocity dispersion suggests that cluster or line-of-sight structures also contribute a substantial fraction of convergence. There is no clear evidence of a crowded environment around the ETG, either by visual inspection of color images or in the SDSS photometric redshifts, but  $\sim 1'$  to the North there is a galaxy, SDSS J142953.71+120333.9, with a BOSS spectroscopic redshift  $z = 0.5527 \pm 0.0002$ , very close to the lensing ETG, indicating that a cluster or group of galaxies at  $z \simeq 0.55$  may be present, as suggested by the external shear field.

For the source, the lens model gives local magnifications of 3.2, 3.1, 1.8 and 0.7 for images A, B, C and D, respectively, which means that the total magnification is  $8.8 \pm 0.4$ . The source has an effective radius  $R_{\text{eff}} = 0''.159 \pm 0''.007$ , which corresponds to  $R_{\text{eff}} = 1.28 \pm 0.06$  kpc for the adopted cosmology. The source has a minor-to-major axis ratio  $q = 0.56$  and Sérsic index  $n = 3.9$ . It is centered at  $\Delta\text{R.A.} = -0''.43$  and  $\Delta\text{Dec.} = 0''.56$  relative to the center of the lens galaxy.

### 3.3. Intrinsic Properties

Having determined the magnification of the LAE we can estimate its intrinsic properties. From the total DECaLS DR2  $r$ -band magnitude, we determine a rest-frame 1600 Å luminosity  $L_{1600} = (6.12 \pm 0.48) \times 10^{30} \text{ erg s}^{-1} \text{ Hz}^{-1}$ . Using the Kennicutt's (1998) conversion, this rest-frame UV luminosity translates into an intrinsic star formation rate (SFR) of  $\simeq 90 M_{\odot} \text{ yr}^{-1}$ , when corrected for magnification, reddening and the lower proportion of low-mass stars in the Chabrier (2003) stellar IMF relative to the standard Salpeter (1955) adopted by Kennicutt (a factor of 1/1.8). Turning to  $\text{Ly}\alpha$ , assuming the space distribution of  $\text{Ly}\alpha$  in the source plane and its lensing magnification are similar to that of the rest-frame UV continuum, and applying the correction for the magnification and the slit losses (the GTC/OSIRIS slit captured a fraction  $\simeq 0.60$  of the total light of BG1429+1202), we derive an intrinsic  $\text{Ly}\alpha$  luminosity  $L_{\text{Ly}\alpha} = (2.80 \pm 0.39) \times 10^{43} \text{ erg s}^{-1}$ . Assuming case-B recombination and the Kennicutt's (1998) conversion, this luminosity translates in a  $\text{SFR}(\text{Ly}\alpha) \simeq 25 M_{\odot} \text{ yr}^{-1}$ . Comparing the estimates of SFR from the rest-frame UV and  $\text{Ly}\alpha$ , we measure  $f_{\text{esc}}^{\text{Ly}\alpha} \sim 0.30$ , consistent with that estimated from LAEs at  $z \sim 3$  (e.g., Zheng et al. 2016; Verhamme et al. 2008). However, we should note that the measured  $f_{\text{esc}}^{\text{Ly}\alpha}$  results from the assumption that the spatial distribution of  $\text{Ly}\alpha$  (and its magnification) follows the rest-frame UV continuum.  $\text{Ly}\alpha$  halos are hard to be resolved from individual LAEs, and have been studied mainly by using stacking techniques (Steidel et al. 2011; Momose et al. 2016), or in nearby high-redshift analogs (e.g. Yang et al. 2016). However, for a few cases, strong gravitational lensing allows spatially resolved studies of high-redshift galaxies (e.g., Patrício et al. 2016). A more detailed analysis will be possible with high-resolution narrow-band imaging and integral field spectroscopy.

In order to establish how typical are the intrinsic properties of this galaxy, we compare it with other UV-selected  $z \sim 3$  LBGs and LAEs. BG1429+1202 is intrinsically more luminous in the rest-frame UV by a factor of 7 and 19, relatively to  $L^*$  from the luminosity functions of Reddy & Steidel (2009) for  $z \sim 3$  LBGs and  $z \sim 3.1$  LAEs selected by narrow-band imaging by Ouchi et al. (2008), respectively. It is also intrinsically very luminous in  $\text{Ly}\alpha$  emission, when compared with  $L_{\text{Ly}\alpha}^*$  from the luminosity functions of LAEs at  $z \sim 3.1$  (factor of  $\sim 5$ ; Ouchi et al. 2008) and LAEs at  $z = 2.8$  in CDFS (factor of  $\sim 9 - 5$ ; Zheng et al. 2016).

A comparison is presented in table 2 with other well known, exceptionally bright in the optical, galaxy-galaxy

$z \sim 3$  lenses: the Cosmic Eye (Smail et al. 2007), MS 1512-cB58 (Yee et al. 1996), the 8 o'clock (Allam et al. 2007), and at lower redshift the Cosmic Horseshoe (Belokurov et al. 2007). BG1429+1202 has similar brightness but is intrinsically very luminous in the rest-frame UV continuum and  $\text{Ly}\alpha$ . It is also the only one  $\text{Ly}\alpha$  emitter (the  $\text{Ly}\alpha$  line of the Cosmic Horseshoe galaxy shares many of the properties of the  $\text{Ly}\alpha$  emitters, but its  $W_0^{\text{Ly}\alpha}$  is below the threshold generally adopted to define it as  $\text{Ly}\alpha$  emitter; Quider et al. 2009). This puts BG1429+1202 in the small group of very bright  $z \sim 3$  galaxies that, due to the high magnification and its high intrinsic luminosity, their brightness provides the unique opportunity to obtain high S/N spectroscopy to study in detail its physical properties.

### 4. CONCLUSION

In this Letter, we report the discovery of a bright quadruply lensed LAE at  $z = 2.8236$ . The very bright apparent magnitude results partially from gravitational lensing by a  $z = 0.5531$  luminous red galaxy, which provides a magnification of  $8.8 \pm 0.4$ . After accounting for the lensing magnification, BG1429+1202 is also intrinsically very luminous in the rest-frame UV and  $\text{Ly}\alpha$  emission by about 19 and 5 times the typical  $L_{\text{UV}}^*$  and  $L_{\text{Ly}\alpha}^*$  of LAEs at  $z \sim 3$ , respectively, showing low dust content and indications of massive recent star formation. Compared with the few well known strongly lensed galaxies, it is the most luminous one in the  $\text{Ly}\alpha$  line. This makes this source another good laboratory for further detailed studies of the physics of star formation and  $\text{Ly}\alpha$  emission in galaxies during the cosmic epoch of star formation. The new method presented in Shu et al. (2016a,b) and in this work opens a new window to the study of high redshift galaxies by the combination of massive spectroscopic surveys, large-area multi-band imaging, gravitational lensing and follow-up with 10 m telescopes like GTC.

We thank the anonymous referee for helpful comments. We thank the IAC Director for the allocation of WHT and GTC discretionary time and the WHT and GTC staff for efficient support and fast completion of the two DDT programs. RMC acknowledges Fundación La Caixa for the financial support received in the form of a PhD contract. This work was funded in part by the project ESP2015-65597-C4-4-R of the Spanish Ministerio de Economía y Competitividad (MINECO). SM and YS acknowledge the support by the Strategic Priority Research Program “The Emergence of Cosmological Structures” of the Chinese Academy of Sciences Grant No. XDB09000000 and by the National Natural Science Foundation of China (NSFC) under grant numbers 11333003, 11390372, and 11603032. Funding for SDSS-III has been provided by the Alfred P. Sloan Foundation, the Participating Institutions, the National Science Foundation, and the U.S. Department of Energy Office of Science. The SDSS-III web site is <http://www.sdss3.org/>.

### REFERENCES

- Allam, S. S., Tucker, D. L., Lin, H., et al. 2007, *ApJ*, 662, L51  
 Belokurov, V., Evans, N. W., Moiseev, A., et al. 2007, *ApJ*, 671, L9



TABLE 2  
INTRINSIC PROPERTIES OF BG1429+1202 AND OTHER BRIGHT GALAXY-GALAXY LENSES

Object	z	$m_{UV}^a$ ( $\simeq 1500 - 1700\text{\AA}$ )	$\mu^b$ ( $\times 10^{29}$ )	$L_{UV}^c$ ( $\text{erg s}^{-1} \text{ Hz}^{-1}$ )	$L_{Ly\alpha}^d$ ( $\times 10^{42} \text{ erg s}^{-1}$ )	Reference
BG1429+1202	2.823	20.16	8.8	6.99	28.0	—
MS 1512-cB58	2.726	20.64	30	1.16	—	1,2
Cosmic Eye	3.073	20.30	28	2.08	—	3
8 o'clock	2.735	19.22	12.3	10.55	—	4
Cosmic Horseshoe	2.381	19.70	24	2.74	3.3	5,6
LBGs	$\sim 3$	24.61	—	1.06	—	7
LAEs	$\sim 3.1$	25.84	—	0.36	5.8	8

NOTE. — (a) rest-frame UV apparent magnitudes from  $r$ - or  $i$ -band, depending on the redshift; (b) total magnification factor; (c) and (d) intrinsic rest-frame UV and  $Ly\alpha$  luminosity, respectively, corrected from the lensing magnification;  
REFERENCES. — (1) Ellingson et al. (1996); (2) Seitz et al. (1998); (3) Smail et al. (2007); (4) Allam et al. (2007); (5) Belokurov et al. (2007); (6) Quider et al. (2009); (7) Reddy & Steidel (2009); (8) Ouchi et al. (2008).

- Benn, C., Dee, K., & Agócs, T. 2008, *Proc. SPIE*, 7014, 70146X  
Bolton, A. S., Burles, S., Koopmans, L. V. E., Treu, T., & Moustakas, L. A. 2006, *ApJ*, 638, 703  
Bolton, A. S., Burles, S., Koopmans, L. V. E., et al. 2008, *ApJ*, 682, 964  
Brownstein, J. R., Bolton, A. S., Schlegel, D. J., et al. 2012, *ApJ*, 744, 41  
Calzetti, D., Armus, L., Bohlin, R. C., et al. 2000, *ApJ*, 533, 682  
Chabrier, G. 2003, *PASP*, 115, 763  
Dahle, H., Aghanim, N., Guennou, L., et al. 2016, *A&A*, 590, L4  
Dawson, K. S., Schlegel, D. J., Ahn, C. P., et al. 2013, *AJ*, 145, 10  
Dessauges-Zavadsky, M., D’Odorico, S., Schaerer, D., et al. 2010, *A&A*, 510, A26  
Eisenstein, D. J., Weinberg, D. H., Agol, E., et al. 2011, *AJ*, 142, 72  
Ellingson, E., Yee, H. K. C., Bechtold, J., & Elston, R. 1996, *ApJ*, 466, L71  
Gaia Collaboration, Brown, A. G. A., Vallenari, A., et al. 2016, *ArXiv e-prints*, arXiv:1609.04172  
Kennicutt, Jr., R. C. 1998, *ApJ*, 498, 541  
Lawrence, A., Warren, S. J., Almaini, O., et al. 2007, *MNRAS*, 379, 1599  
Lin, H., Buckley-Geer, E., Allam, S. S., et al. 2009, *ApJ*, 699, 1242  
Newville, M., Stensitzki, T., Allen, D. B., & Ingargiola, A. 2014, *LMFIT: Non-Linear Least-Square Minimization and Curve-Fitting for Python*, doi:10.5281/zenodo.11813  
Momose, R., Ouchi, M., Nakajima, K., et al. 2016, *MNRAS*, 457, 2318  
Ouchi, M., Shimasaku, K., Akiyama, M., et al. 2008, *ApJS*, 176, 301  
Patrício, V., Richard, J., Verhamme, A., et al. 2016, *MNRAS*, 456, 4191  
Peng, C. Y., Ho, L. C., Impey, C. D., & Rix, H.-W. 2002, *AJ*, 124, 266  
Pettini, M., Steidel, C. C., Adelberger, K. L., Dickinson, M., & Giavalisco, M. 2000, *ApJ*, 528, 96  
Pettini, M., Rix, S. A., Steidel, C. C., et al. 2002, *ApJ*, 569, 742  
Quider, A. M., Pettini, M., Shapley, A. E., & Steidel, C. C. 2009, *MNRAS*, 398, 1263  
Quider, A. M., Shapley, A. E., Pettini, M., Steidel, C. C., & Stark, D. P. 2010, *MNRAS*, 402, 1467  
Reddy, N. A., & Steidel, C. C. 2009, *ApJ*, 692, 778  
Salpeter, E. E. 1955, *ApJ*, 121, 161  
Schlafly, E. F., & Finkbeiner, D. P. 2011, *ApJ*, 737, 103  
Seitz, S., Saglia, R. P., Bender, R., et al. 1998, *MNRAS*, 298, 945  
Shapley, A. E., Steidel, C. C., Pettini, M., & Adelberger, K. L. 2003, *ApJ*, 588, 65  
Shu, Y., Bolton, A. S., Brownstein, J. R., et al. 2015, *ApJ*, 803, 71  
Shu, Y., Bolton, A. S., Kochanek, C. S., et al. 2016a, *ApJ*, 824, 86  
Shu, Y., Bolton, A. S., Mao, S., et al. 2016b, *ArXiv e-prints*, arXiv:1608.08707  
Shu, Y., Bolton, A. S., Moustakas, L. A., et al. 2016c, *ApJ*, 820, 43  
Smail, I., Swinbank, A. M., Richard, J., et al. 2007, *ApJ*, 654, L33  
Steidel, C. C., Bogosavljević, M., Shapley, A. E., et al. 2011, *ApJ*, 736, 160  
Verhamme, A., Schaerer, D., Atek, H., & Tapken, C. 2008, *A&A*, 491, 89  
Yang, H., Malhotra, S., Rhoads, J. E., et al. 2016, *ArXiv e-prints*, arXiv:1610.05767  
Yee, H. K. C., Ellingson, E., Bechtold, J., Carlberg, R. G., & Cuillandre, J.-C. 1996, *AJ*, 111, 1783  
York, D. G., Adelman, J., Anderson, Jr., J. E., et al. 2000, *AJ*, 120, 1579  
Zheng, Z.-Y., Malhotra, S., Rhoads, J. E., et al. 2016, *ApJS*, 226, 23